Available online at www.sciencedirect.com
ScienceDirect
Catalysis Today 129 (2007) 322–329
CATALYSIS TODAY
www.elsevier.com/locate/cattod

Novel zirconia-supported catalysts for low-temperature oxidative steam reforming of ethanol

Jia-Lin Bi [a,b], Yeh-Yeau Hong [a,b], Chia-Chan Lee [a,b], Chuin-Tih Yeh [b], Chen-Bin Wang [a,*]

[a] *Department of Applied Chemistry, Chung Cheng Institute of Technology, National Defense University, Tahsi, Taoyuan 33509, Taiwan, ROC*
[b] *Department of Chemical Engineering and Materials Science, Yuan Ze University, Chungli, Taoyuan, Taiwan, ROC*

Available online 19 September 2007

Abstract

Three zirconia-supported platinum group metal (Pt, Ru and Pt–Ru) catalysts were prepared by impregnation. The activity of these catalysts toward the oxidative steam reforming of ethanol (OSRE) was examined in a fixed-bed reactor in the temperature range of 260–380 °C. The catalysts were characterized by X-ray diffraction (XRD), temperature-programmed reduction (TPR), transmission electron microscopy (TEM) and nitrogen adsorption at −196 °C. Activity results indicated that the optimized experimental conditions involved a reforming temperature of close to 300 °C and the molar ratios of O_2/EtOH and H_2O/EtOH of 0.44 and 4.9, respectively. An ethanol conversion (C_{EtOH}) approaching 100% and a hydrogen yield (Y_{H_2}) exceeding 3.0 mole/mole ethanol were noticed at 280 °C over all the catalysts. Among these catalysts, the Pt–Ru/ZrO_2 catalyst was an excellent OSRE catalyst at low temperature. The maximum Y_{H_2} was 4.4 and the CO distribution was 3.3 mol% at 340 °C.

Keywords: Ethanol; Oxidative steam reforming; PEMFCs

1. Introduction

Hydrogen is a potentially clean energy source for the highly efficient generation of electricity through fuel cell systems. Among various liquid fuels, the candidate for the hydrogen source is ethanol [1]. Ethanol is a favorable source of hydrogen, because it can be obtained from renewable sources, including biomass [2]. Meanwhile, it is inexpensive, easy to handle and transport, biodegradable and less toxic [3]. Another advantage of ethanol over fossil fuels involves the neutralization of carbon [4].

Hydrogen can be produced directly from ethanol by different processes such as steam reforming of ethanol (SRE, Eq. (1)) [5–10], partial oxidation of ethanol (POE, Eq. (2)) [11–13] and oxidative steam reforming of ethanol (OSRE or autothermal reforming, Eq. (3)) [14–23]:

$$C_2H_5OH_{(l)} + 3H_2O_{(l)} \rightarrow 6H_{2(g)} + 2CO_{2(g)}, \quad \Delta H_{298}{}^{\circ} = +347.4\,\text{kJ/mol} \qquad (1)$$

$$C_2H_5OH_{(l)} + (3/2)O_{2(g)} \rightarrow 3H_{2(g)} + 2CO_{2(g)}, \quad \Delta H_{298}{}^{\circ} = -557.2\,\text{kJ/mol} \qquad (2)$$

$$C_2H_5OH_{(l)} + 1.78H_2O_{(l)} + 0.61O_{2(g)} \rightarrow 4.78H_{2(g)} + 2CO_{2(g)}, \quad \Delta H_{298}{}^{\circ} = 0\,\text{kJ/mol} \qquad (3)$$

The SRE requires a large amount of heat to maintain a reaction temperature of $T_R > 600$ °C. SRE reaction has been performed recently over nickel, cobalt, nickel/copper and noble metals such as palladium, platinum and rhodium on different supports [5,8,9,24,25]. High-temperature reforming preferentially produces a considerable amount of CO which poisons the PEMFCs. Therefore, H_2-rich gas must undergo purification by CO oxidation downstream before being fed into the fuel cell. POE reaction is an exothermic reaction that has been recently described as a method for producing H_2 by Ni–Fe catalysts [11]. The reaction forms hot-spots [26], but could be performed at a lower temperature (about 300 °C). Recently, OSRE reaction has been considered that combines the benefits of both SRE and POE by co-feeding oxygen, steam and ethanol. Verykios et al. used supported Ru and Ni catalysts, and a Rh/CeO_2 catalyst [14–16] to convert ethanol and a hydrogen selectivity (S_{H_2}) of 100% was

* Corresponding author. Fax: +886 33 891519.
E-mail address: chenbin@ccit.edu.tw (C.-B. Wang).

0920-5861/$ – see front matter © 2007 Elsevier B.V. All rights reserved.
doi:10.1016/j.cattod.2006.11.027

achieved at 700 °C. Navarro et al. studied a series of Pt catalysts supported on alumina modified by Ce and/or La [17]. Song et al. reformed ethanol to produce H_2 over Ni–Rh/CeO_2 catalysts at temperatures of under 400 °C [18]. Fierro et al. investigated OSRE over Ni-based catalysts and obtained 100% S_{H_2} but with an S_{CO} of over 75% [19]. Velu et al. reformed ethanol to yield 2.5–3.5 mole(H_2 yield)/mole ethanol over CuNiZnAl mixed oxide catalysts at temperatures of under 300 °C [20,21]. The OSRE reaction is very interesting, as it improves ethanol conversion and H_2/CO selectivity over those achieved using SRE. Noble metal catalysts are very efficient in the reforming of ethanol to generate H_2 and CO/CO_2 [6,27,28]. The nature of the support is also important to the selectivity of H_2 formation. Acidic supports, such as Al_2O_3 are known to preferentially dehydrate, while basic supports such as MgO favor dehydrogenation and condensation [6,10]. Reducible oxides, such as ZrO_2 and CeO_2 are expected to offer improved catalytic performance with high selectivity to H_2 and low selectivity to undesirable by-products. Based on the reducibility [29], thermal stability [30,31], adsorption promotion and CO oxidation capabilities [29,32], we chose ZrO_2 support in this study. The effect of CeO_2 and CeO_2–ZrO_2 mixed oxide supports will be discussed in the near future.

In this work, the OSRE reaction is investigated over zirconia-supported platinum group metals (Pt, Ru and Pt–Ru). Therefore, the aim of this work centers on developing a very efficient and more stable catalyst for the on-board reforming of ethanol at relatively lower temperatures in order to generate H_2 with high selectivity and low CO in the outlet gas.

2. Experimental

2.1. Catalyst preparation

A sol–gel method was used for the preparation of ZrO_2 support using $Zr[O(CH_2)_3CH_3]_4$ (Strem) as precursor. It was thoroughly dissolved in ethanol and the solution was gelatized with deionized water. After drying at 100 °C and calcination at 400 °C, prepared ZrO_2 powder was stored as support.

Zirconia-supported catalysts (Pt, Ru and Pt–Ru/Pt/ZrO_2) were prepared with impregnating the supports by using H_2PtCl_6 and $RuCl_3$ as precursors. The loading of both Pt/ZrO_2 and Ru/ZrO_2 catalysts were 3 wt.%, Pt–Ru/ZrO_2 catalyst was 1.5 wt.% for each component, respectively. After drying at 380 °C and calcination at 400 °C, prepared samples were crashed to 60–80 mesh and stored as fresh catalysts. Platinum loadings in the fresh catalysts were determined by the atomic-emission technique using an ICP-MS (Perkin-Elmer).

2.2. Catalyst characterization

Nitrogen adsorption isotherms at −196 °C were determined volumetrically with NOVA 4200e accelerated surface area and porosimetry analyzer. In each test, approximately 0.25 g of fresh sample was pre-outgassed under 5×10^{-5} Torr for 3 h at 110 °C. The surface area was calculated from the nitrogen adsorption isotherm. Results of physical characterization of supported catalysts obtained are summarized in Table 1.

Table 1
Surface area and metal content of ZrO_2-supported catalysts

Catalysts	S_{BET} (m^2/g)	Metal content (wt.%)[a]
ZrO_2	130	–
Pt/ZrO_2	103	Pt: 2.52
Ru/ZrO_2	128	Ru: 1.64
Pt–Ru/ZrO_2	96	Pt: 1.36; Ru: 1.18

[a] Measured by ICP-AES.

Powder X-ray diffraction patterns (XRD) were obtained using a Shimadzu XRD-6000 diffractometer with a Ni-filtered Cu Kα radiation from 20° to 80° at a rate of 0.05°/s. Spectra were collected after catalyst calcinations. The microstructure and particle size of the reduced catalysts was observed, using transmission electron microscopy (TEM) with a JEM-2010 microscope (JEOL), at an acceleration voltage of 200 kV.

Reduction behavior of zirconia-supported platinum group metals was studied by temperature-programmed reduction (TPR). About 50 mg of the sample was heated in a flow of 10% H_2/N_2 gas mixture at a flow rate of 10 ml min^{-1}. During TPR, the temperature was programmed to rise with 7 °C/min from −80 to 190 °C. The amount of the consumed H_2 was monitored continuously with a thermal conductivity detector (TCD).

2.3. Catalytic activity measurement

Catalytic activities of prepared samples towards OSRE reaction were tested in a fixed-bed flow reactor at atmospheric pressure. Catalyst of 100 mg was placed in a 4 mm i.d. quartz tubular reactor and held by glass-wool plugs. Before reaction, the catalyst was activated by reduction with hydrogen at 200 °C for 3 h. Temperature of the reactor was controlled by a heating tape and measured by a thermocouple (1.2 mm i.d.) at the center of the reactor bed. The gas hourly space velocity (GHSV) was maintained at 66,000 h^{-1}. The optimal molar ratios of O_2/EtOH and H_2O/EtOH for the OSRE reaction were tuned to understand the role of oxidants in the catalysis of the OSRE reaction. OSRE activity was tested stepwise by increasing the temperature from 260 to 380 °C. A 5 h of reaction time was maintained for each reaction temperature. Within the specified temperature range, oxygen was completely consumed.

The reaction products were separated with columns of Porapak Q (for CO_2, H_2O, C_2H_4, CH_3CHO, CH_3OCH_3 and EtOH) and Molecular Sieve 5A (for H_2, O_2, CH_4 and CO) and quantitatively analyzed by two sets of TCD-GC on line. Major products were H_2, CO_2, CO and CH_4. Trace amount (lower than 0.5 mol%) of CH_3CHO has been detected as by-product. The evaluation of OSRE activity and the selectivity of all samples depend on conversion of ethanol (C_{EtOH}), the distribution of products (mol%) and yield of hydrogen (Y_{H_2}). Both the C_{EtOH} and Y_{H_2} in the OSRE reactions were calculated according to following equations:

$$C_{EtOH} = \frac{n_{EtOH\text{-}in} - n_{EtOH\text{-}out}}{n_{EtOH\text{-}in}} \times 100\% \quad (4)$$

$$Y_{H_2} = \frac{n_{H_2\text{-}out}}{[(1/2)(n_{CH_4\text{-}out} + n_{CO\text{-}out} + n_{CO_2\text{-}out})] + n_{C_2H_4O\text{-}out}} \quad (5)$$

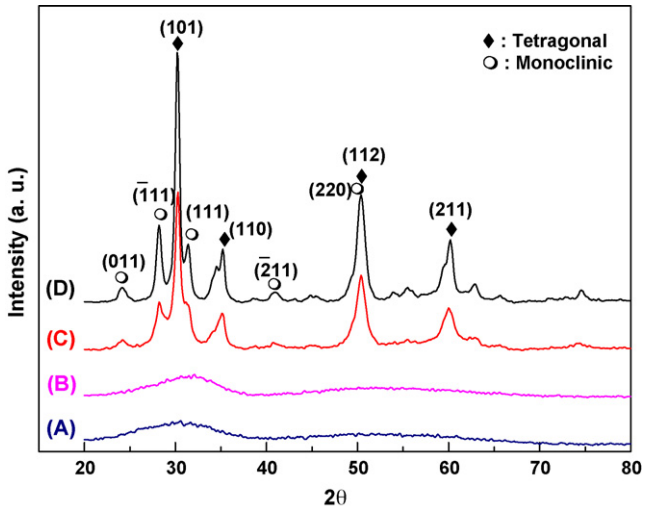

Fig. 1. XRD patterns of ZrO_2 support: (A) as-prepared, (B) calcined at 200 °C, (C) calcined at 400 °C and (D) calcined at 600 °C.

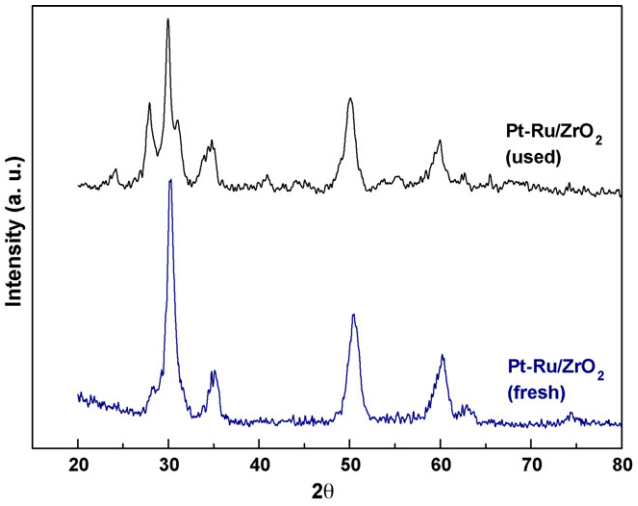

Fig. 2. XRD patterns of fresh and used Ru/ZrO_2 catalyst.

3. Results and discussion

3.1. Characteristic analysis

Table 1 summarizes the surface area and noble metal content of the catalyst in this study. The surface area (S_{BET}) of the self-prepared ZrO_2 by the sol–gel method is higher than that of commercial ZrO_2. The S_{BET} declines slowly as the metal loading increases.

X-ray diffraction is employed to identify the crystalline phases in the catalysts. Fig. 1 shows the XRD patterns of as-prepared ZrO_2 and calcined derivatives (at 200, 400 and 600 °C). A broad peak in the 2θ range of 20–40° (Fig. 1A and B) reveals that the as-prepared zirconia and the derivative under 200 °C calcined are amorphous. As the calcined temperature approaches 400 °C (Fig. 1C), mixed phase are formed. The diffraction peaks at 30°, 34.5°, 50° and 60° are associated with the tetragonal structure. Other diffraction peaks (24°, 28°, 32° and 41°) reveal the monoclinic structure. The broad peaks under 400 and 600 °C calcination (Fig. 1C and D) indicate the small size of the nano-crystallite. Fig. 2 displays the XRD patterns of fresh and used (under 280 °C, 72 h) $Pt–Ru/ZrO_2$ catalyst. No significant diffraction signal of Pt(1 1 1) or PtRu(1 1 1) is observed for either the fresh or the used catalyst, perhaps the corresponding particles on ZrO_2 supports are below the detection limit of XRD. However, the increase in the peak intensities of the monoclinic phase and decrease in the tetragonal phase show that the OSRE reactive atmosphere and reaction temperature (280 °C) can cause the transformation of the zirconia phases.

Fig. 3A, C and E shows TEM images of three reduced catalysts. Clearly, the grain sizes of ZrO_2 support are around 20 nm. The particle size distribution was determined by directly measuring the sizes of 100 particles from magnified TEM photographs presented in Fig. 3B, D and F. The obtained histograms are analyzed from many parts of the TEM photographs. The mean diameters of the particles are 1.7, 1.4 and 1.4 nm for $Pt–Ru/ZrO_2$, Pt/ZrO_2 and Ru/ZrO_2, respectively.

The redox properties of the catalysts are studied by TPR and presented in Figs. 4 and 5. All fresh samples are preferentially reduced at 200 °C for 3 h to eliminate the interference of coordinated chloride ion. Further, the reduced samples are re-oxidized at different temperatures (assigned as O_T). Fig. 4 shows TPR characterizations of $Pt–Ru/ZrO_2$, Pt/ZrO_2 and Ru/ZrO_2 catalysts that re-oxidize at 25 °C, and of the self-prepared ZrO_2 support. No TPR trace for the ZrO_2 support in the temperature range −80 to 180 °C is shown. The TPR trace of the Ru/ZrO_2 catalyst exhibits two peaks, at $T_{r1} = 84$ °C and $T_{r2} = 112$ °C (T_{r1} and T_{r2} are the temperatures of reduction). Imamura et al. [33] noticed two reduction peaks for Ru/CeO_2 catalyst and suggested that the peak of lower temperature attributed to the well-dispersed Ru species and the higher temperature of well-crystallized RuO_2. Comparison with this literature, the two species associated with T_{r1} and T_{r2} are assigned as Ru^dO_2 (well-dispersed RuO_2) and Ru^cO_2 (crystallized RuO_2), respectively. Both Pt/ZrO_2 and $Pt–Ru/ZrO_2$ catalysts show broad peaks in the temperature range −50 to 100 °C. Sachtler et al. [34] and Hwang and Yeh [35] reported that Pt^sO (surface platinum oxide) in Pt/SiO_2 sample is reduced below 20 °C. The variation of the reduction temperature may be related to the difference in environments or Pt^sO particle sizes. The results herein demonstrate that the trace of the Pt/ZrO_2 sample can be assigned to the reduction of Pt^sO ($T_r \sim 10$ °C) and the surface mixed Pt^{2+}–Zr^{4+} phase (which is difficult to reduce, with $T_r \sim 20$–100 °C). The trace of the $Pt–Ru/ZrO_2$ sample is attributable to the reduction of Pt^sO ($T_r \sim -30$ °C), Pt^aRuO_x (defined as the oxide of the Pt-rich alloy, $T_r \sim 25$ °C) and Ru^dO_2 ($T_r \sim 65$ °C). A comparison of these TPR traces reveals that the T_r of $Pt–Ru/ZrO_2$ is lower than those of Pt/ZrO_2 and Ru/ZrO_2, perhaps because the formation of PtRu alloy, which shifts the reduction temperatures.

Fig. 5 shows TPR characterizations of the $Pt–Ru/ZrO_2$ sample re-oxidized at different temperatures (25, 50, 100 and 200 °C, which are assigned as O_{25}, O_{50}, O_{100} and O_{200},

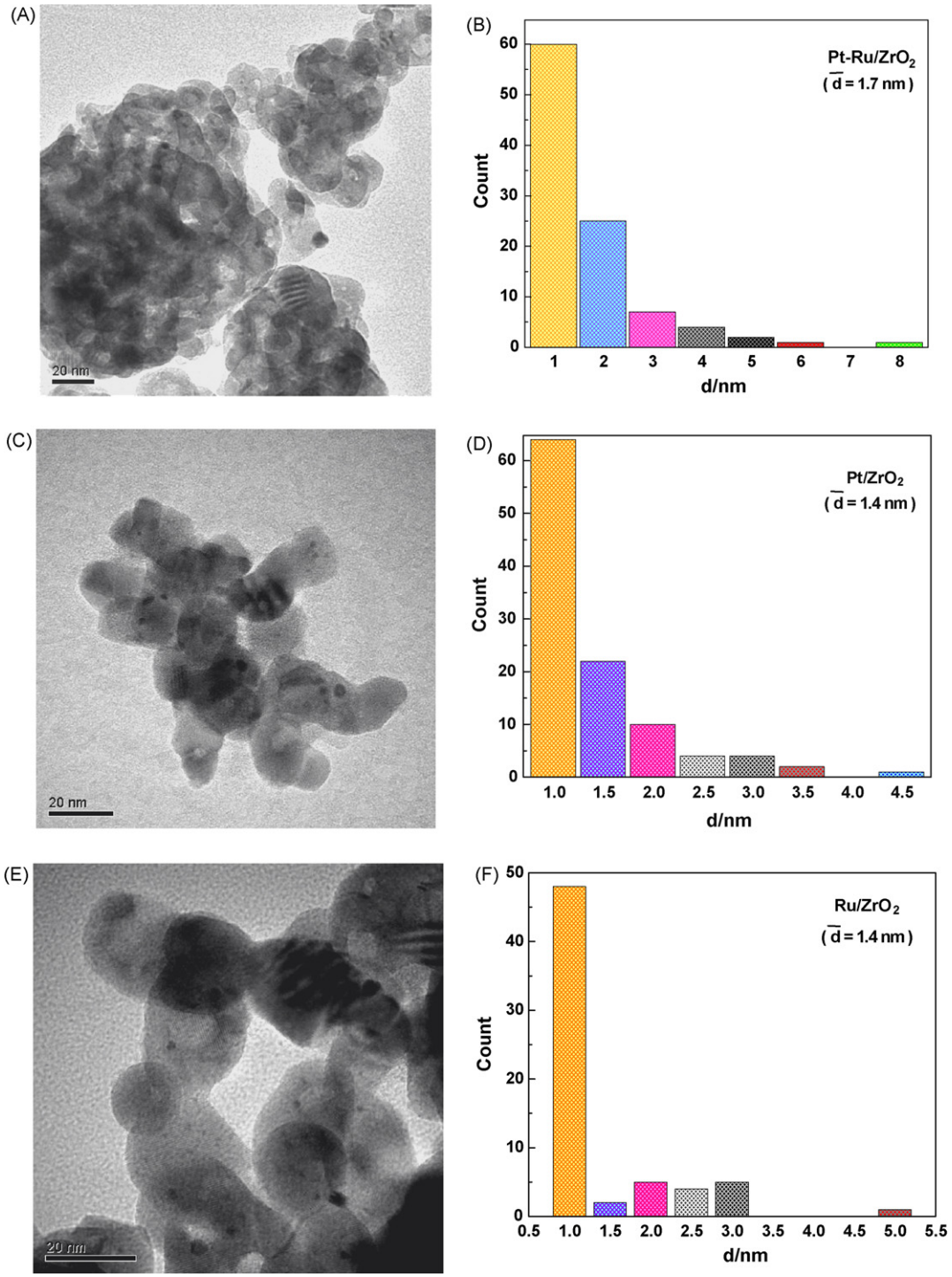

Fig. 3. TEM micrograph of ZrO_2-supported catalyst: (A and B) Pt–Ru/ZrO_2 catalyst, (C and D) Pt/ZrO_2 catalyst and (E and F) Ru/ZrO_2 catalyst.

respectively). These traces have five main peaks at various reduction temperatures. They are assigned to species Pt^sO (T_r: −30 to 0 °C), Pt^aRuO_x (T_r: 20–50 °C), Ru^dO_2 (T_r: 60–70 °C), $PtRu^aO_x$ (defined as the oxide of Ru-rich alloy, T_r: 60–90 °C) and Ru^cO_2 (T_r: 70–100 °C), respectively. As the O_T is increased, the abundance of the Pt^sO and Ru^dO_2 species gradually decreases and the dominant species (Pt^aRuO_x and Ru^cO_2) alternate. Since the migration of Ru to the PtRu alloy surface increases with O_T, species $PtRu^aO_x$ and Ru^cO_2 become the major species when the reduced Pt–Ru/ZrO_2 sample is re-oxidized at 100 and 200 °C.

3.2. Catalytic ethanol reforming

3.2.1. Effect of O_2/EtOH

Verykios et al. [14,15] performed OSRE research separately using a ruthenium catalyst and a nickel catalyst under molar ratios of O_2/EtOH = 0.61 and H_2O/EtOH = 3. Song et al. [18]

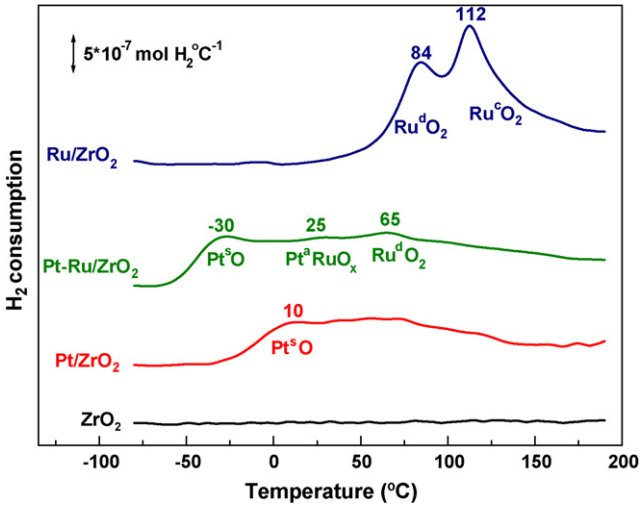

Fig. 4. TPR profiles of ZrO_2, Pt/ZrO_2, $Pt–Ru/ZrO_2$ and Ru/ZrO_2 catalysts after re-oxidation at 25 °C.

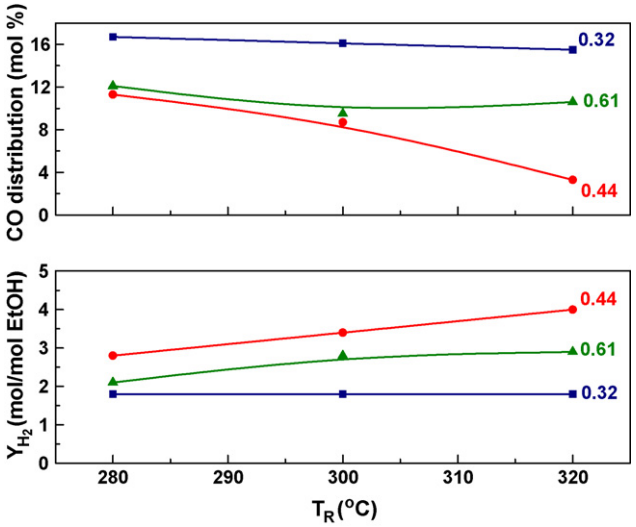

Fig. 6. Effect of O_2/EtOH for OSRE reaction with various temperatures over $Pt–Ru/ZrO_2$ catalyst.

studied the OSRE reaction with a series of $Rh–Ni/CeO_2$ catalysts under molar ratios of O_2/EtOH = 0.4 and H_2O/EtOH = 4. In this part, a molar ratio of H_2O/EtOH = 4.9 is fed into the reactor and a series of O_2/EtOH molar ratios of 0.32, 0.44 and 0.61 are tuned separately for $Pt–Ru/ZrO_2$ sample. The C_{EtOH} approaches 100% under these conditions at around 280 °C. The results shown in Fig. 6 indicate that the decreasing O_2/EtOH ratio tends to increase the amount of by-products (CH_4 and CO) and decrease the Y_{H_2} in the range 280–320 °C. However, the increasing of O_2/EtOH ratio tends to favor the combustion of hydrogen and drop in Y_{H_2}. According to the tuning experiments, the optimized O_2/EtOH molar ratio is found to be 0.44. Under this condition, both the CO decreases and Y_{H_2} increases with the increasing reaction temperature (T_R).

3.2.2. Effect of H_2O/EtOH

Subsequently, an O_2/EtOH molar ratio of 0.44 was fed into the reactor and a series of H_2O/EtOH molar ratios of 13, 4.9, 2.2 and 0.8 are tuned separately for $Pt–Ru/ZrO_2$ sample. The C_{EtOH} approaches 100% under these conditions at around 280 °C. Fig. 7 shows that the light-off temperature of ethanol is shifted to 350 °C for the H_2O/EtOH molar ratios of 2.2 and 0.8. Since the lower H_2O/EtOH ratios promote the POE reaction that evolves a large amount of heat. Therefore, T_R could not fall below 350 °C. The feed with lower ethanol concentration (i.e., H_2O/EtOH = 13) has a low T_R because the light-off exothermic heat is absorbed by the water, producing more CO than any other molar ratios of H_2O/EtOH. Meanwhile, the effect of H_2O/EtOH molar ratio of 4.9 on the catalysis of the OSRE reaction is predominant that decreases the amount of CO and increases the amount of Y_{H_2} conspicuously in the range 280–320 °C.

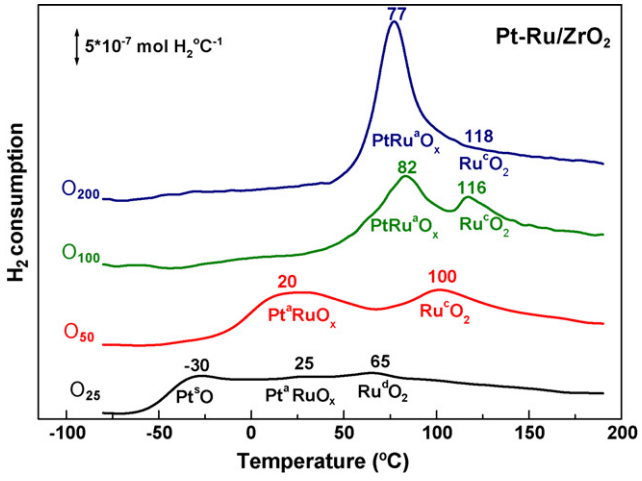

Fig. 5. TPR profiles of $Pt–Ru/ZrO_2$ catalyst after re-oxidation at different temperatures.

3.2.3. Effect of reaction temperature

The above results reveal that controlling the OSRE reaction at low temperatures can avoid methanation (at a moderate

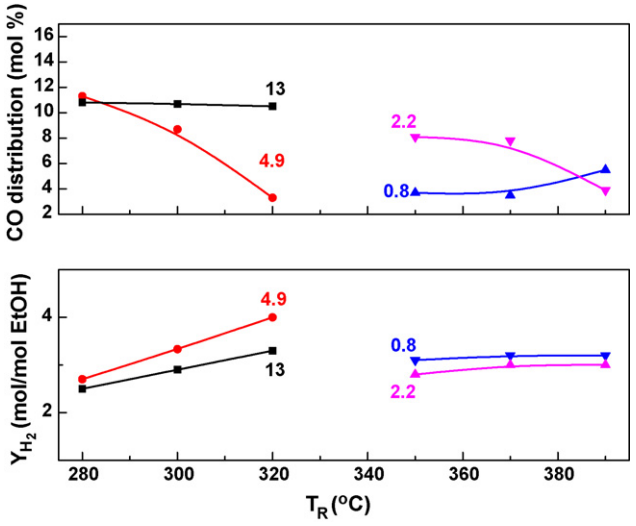

Fig. 7. Effect of H_2O/EtOH for OSRE reaction with various temperatures over $Pt–Ru/ZrO_2$ catalyst.

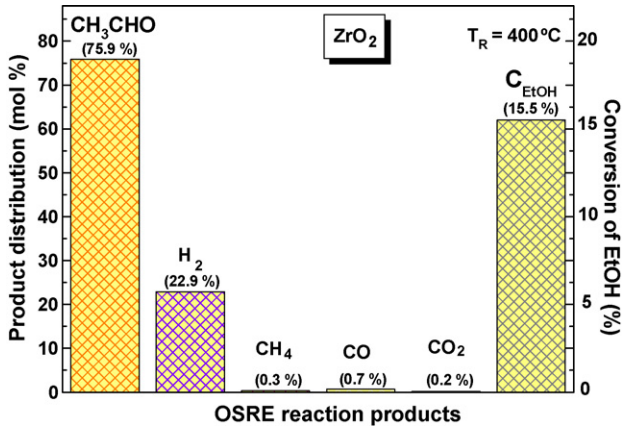

Fig. 8. Conversion of ethanol and products distribution towards the OSRE reaction over ZrO_2 support at 400 °C under O_2/EtOH = 0.44, H_2O/EtOH = 4.9 and GHSV = 66,000 h^{-1}.

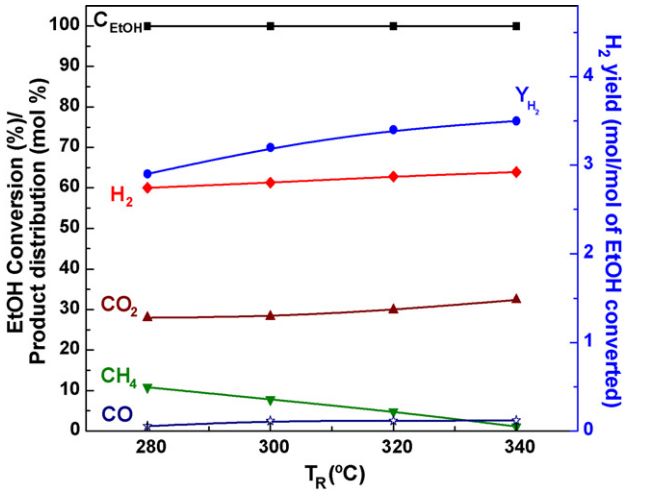

Fig. 9. Catalytic performance in the OSRE reaction over Pt/ZrO_2 catalyst under O_2/EtOH = 0.44, H_2O/EtOH = 4.9 and GHSV = 66,000 h^{-1}.

temperature of ~500 °C) [19,36–38] and the formation of a large amount of CO (at a high temperature of ~700 °C) [19,36–38]. The optimized molar ratios of O_2/EtOH and H_2O/EtOH feeds are 0.44 and 4.9, respectively at 280–340 °C.

In order to understand the catalytic performance of zirconia support, a blank experiment is analyzed. Fig. 8 displays the C_{EtOH} and distribution of products towards the OSRE reaction over ZrO_2 at 400 °C. Pure ZrO_2 exhibits weak activity (C_{EtOH} approaches 16%) at this temperature. The main product is CH_3CHO and small amounts of by-products (CH_4, CO and CO_2) are formed. The distributions are attributed to the almost complete dehydrogenation of ethanol and the slight decarbonylation of acetaldehyde over pure ZrO_2:

$$CH_3CH_2OH \rightarrow CH_3CHO + H_2 \quad (6)$$

$$CH_3CHO \rightarrow CO + CH_4 \quad (7)$$

The cleavage of the C–C bond is a very important step in the reforming of ethanol. Both platinum and ruthenium can cleave the C–C bond [39]. The catalytic activity is significantly enhanced when the zirconia support is impregnated with platinum group metals. Therefore, the three catalysts can completely convert the ethanol at low temperatures with a trace amount of CH_3CHO formation (since the CH_3CHO is easily converted to CH_4 and CO via Eq. (7)). Figs. 9–11 exhibit the catalytic performance in the OSRE reaction over three catalysts at 280–340 °C. Ethanol is completely converted over the entire temperature range. The distribution of H_2 and CO_2 products increases with temperature, whereas CH_4 and CO decrease over Pt/ZrO_2 catalyst (Fig. 9). The Pt [40–42] and Ru [43–46] catalysts can preferentially oxidize CO in the presence of hydrogen. The results show that the CO distribution over Pt/ZrO_2 is the lowest (1–2.6 mol%) among the three catalysts. The CH_4 distribution is highest (10.8 mol%) over Pt/ZrO_2 at 280 °C and declines with an increasing temperature. Based on these observations of the Pt/ZrO_2 catalyst, the CO oxidation (Eq. (8)) is dominant at low temperature (280 °C). The drop in the concentration of CH_4 and the increase in the concentration of H_2 with temperature are attributable to the steam reforming of methane (Eq. (9)):

$$CO + (1/2)O_2 \rightarrow CO_2 \quad (8)$$

$$CH_4 + H_2O \rightarrow CO + 3H_2 \quad (9)$$

The distribution of H_2 and CO_2 products increases with temperature, whereas the products of CH_4 and CO decrease as the temperature increase over 300 °C on Ru/ZrO_2 catalyst (Fig. 10). These results reveal that the water gas shift (WGS, Eq. (11)) reaction is preferential over Ru/ZrO_2 catalyst to reduce the amount of CO:

$$CO + H_2O \rightarrow CO_2 + H_2 \quad (10)$$

The CO distribution over Pt–Ru/ZrO_2 catalyst is highest (9.4 mol%) at 280 °C (Fig. 11). However, the amount of CH_4 (1.8 mol%) is lowest among the three catalysts indicating that the steam reforming of methane can occur at low temperature over Pt–Ru/ZrO_2 catalyst. Therefore, Y_{H_2} is the highest for this catalyst over the entire temperature range. A further investigation

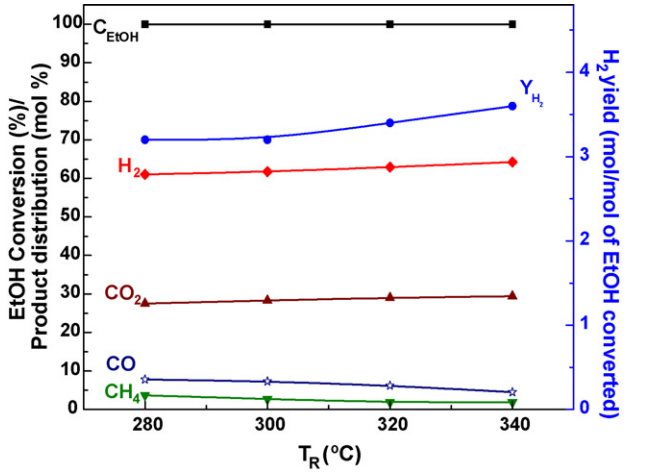

Fig. 10. Catalytic performance in the OSRE reaction over Ru/ZrO_2 catalyst under O_2/EtOH = 0.44, H_2O/EtOH = 4.9 and GHSV = 66,000 h^{-1}.

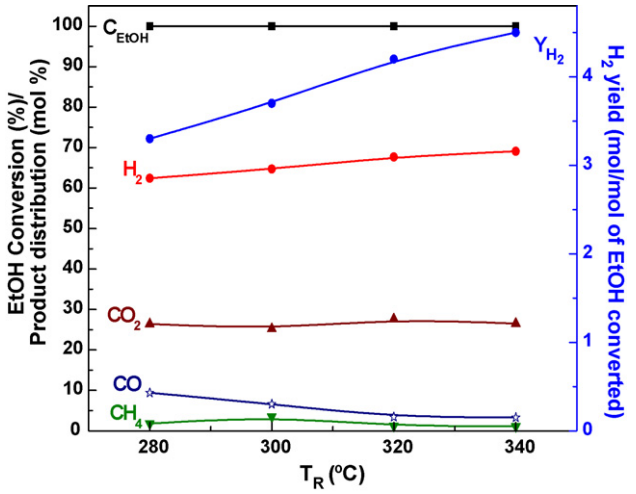

Fig. 11. Catalytic performance in the OSRE reaction over Pt–Ru/ZrO_2 catalyst under O_2/EtOH = 0.44, H_2O/EtOH = 4.9 and GHSV = 66,000 h^{-1}.

of the catalyst stability in a time-on-stream experiment over Pt–Ru/ZrO_2 catalyst at 280 °C is performed under O_2/EtOH = 0.44, H_2O/EtOH = 4.9 and GHSV = 66,000 h^{-1}. This catalyst did not noticeably decay over 72 h. Based on the characterization of TPR over the temperature range of interest, the $PtRu^aO_x$ and Ru^cO_2 species are present on the Pt–Ru/ZrO_2 catalyst surface that promote the cleavage of C–C bond, the steam reforming of methane and the WGS reactions. The maximum Y_{H_2} is 4.4 and the CO distribution is 3.3 mol% under 340 °C.

According to the characterizations and measurements of activity, a reaction scheme (Fig. 12) that includes all significant reaction pathways is proposed for OSRE over Pt–Ru/ZrO_2 catalyst (no including the steam reforming of methane and WGS reactions). Based on the review of literatures [36,47–50], we summarize these reactions involved in the adsorption and decomposition of EtOH as follows:

(1) Sequential elimination of hydrogen:

$$CH_3CH_2OH_{(a)} \rightarrow CH_3CH_2O_{(a)} + H_{(a)} \quad (11)$$

$$CH_3CH_2O_{(a)} \rightarrow CH_3CHO_{(a)} + H_{(a)} \quad (12)$$

$$CH_3CHO_{(a)} \rightarrow CH_3CO_{(a)} + H_{(a)} \quad (13)$$

(2) Cleavage of C–C bond:

$$CH_3CO_{(a)} \rightarrow CH_{3(a)} + CO_{(a)} \quad (14)$$

(3) Products formation:

$$CH_{3(a)} + H_{(a)} \rightarrow CH_{4(g)} \quad (15)$$

$$CO_{(a)} \rightarrow CO_{(g)} \quad (16)$$

$$CO_{(a)} + O_{(a)} \rightarrow CO_{2(g)} \quad (17)$$

$$2H_{(a)} \rightarrow H_{2(g)} \quad (18)$$

4. Conclusion

A new Pt–Ru bimetallic catalyst supported on a ZrO_2 with a high-surface area was successfully synthesized and the optimal O_2/EtOH and H_2O/EtOH molar ratios were determined. At these molar ratios, the OSRE reaction helped to yield H_2-rich gas at a relatively low temperature. This investigation clearly indicates that the OSRE reaction is more efficient at a lower

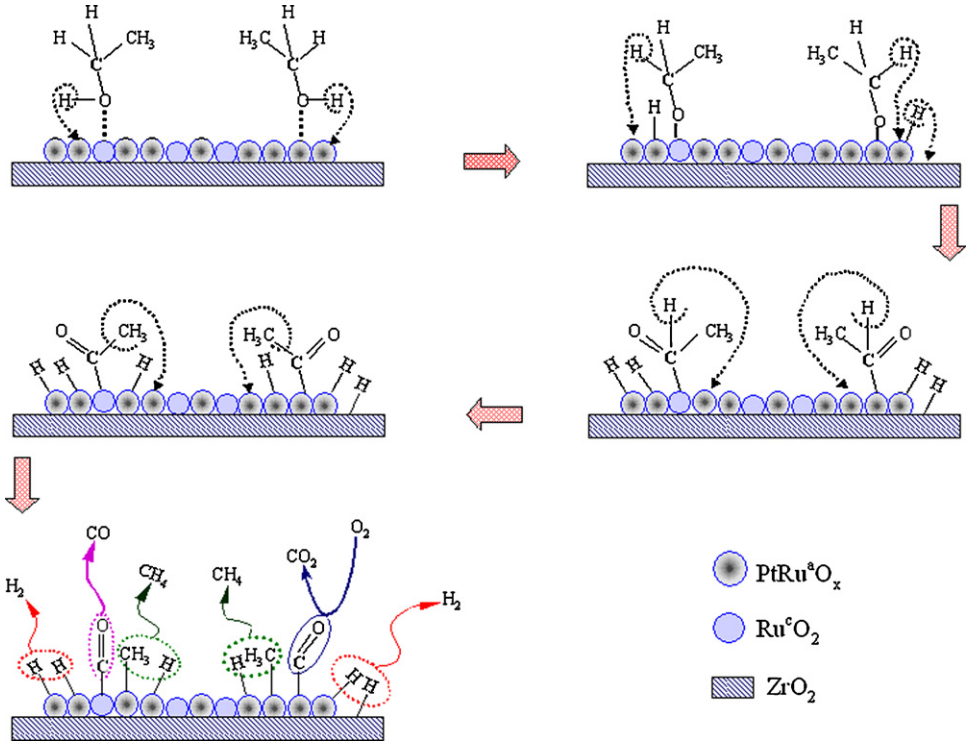

Fig. 12. The reaction scheme for OSRE over Pt–Ru/ZrO_2 catalyst.

operating temperature (around 300 °C) for producing mainly a mixture of H_2 and CO_2 with lower distributions towards undesirable CO and CH_3CHO and with an ethanol conversion of 100%. Among these catalysts, the Pt–Ru/ZrO_2 catalyst was an excellent OSRE catalyst of the production of hydrogen at low temperature. The maximum Y_{H_2} was 4.4 and the CO distribution was 3.3 mol% at 340 °C.

Acknowledgement

The authors would like to thank the National Science Council of the Republic of China, Taiwan, for financially supporting this research under contract no. NSC 94-2113-M-014-002.

References

[1] A. Midilli, M. Ay, I. Dincer, M.A. Rosen, Renew. Sust. Energy Rev. 9 (2005) 273.
[2] T. Ioannides, J. Power Sources 92 (2001) 17.
[3] S. Freni, J. Power Sources 94 (2001) 14.
[4] V. Klouz, V. Fierro, P. Denton, H. Katz, J.P. Lisse, S. Bouvot-Mauduit, C. Mirodatos, J. Power Sources 105 (2002) 26.
[5] A.N. Fatsikostas, D.I. Kondarides, X.E. Verykios, Chem. Commun. (2001) 851.
[6] J.P. Breen, R. Burch, H.M. Coleman, Appl. Catal. B: Environ. 39 (2002) 65.
[7] J. Llorca, P.R. Piscina, J. Sales, N. Homs, Chem. Commun. (2001) 641.
[8] F. Haga, T. Nakajima, K. Yamashita, S. Mishima, React. Kinet. Catal. Lett. 63 (1998) 253.
[9] D. Srinivas, C.V.V. Satyanarayana, H.S. Potdar, P. Ratnasamy, Appl. Catal. A: Gen. 246 (2003) 323.
[10] D.K. Liguras, D.I. Kondarides, X.E. Verykios, Appl. Catal. B: Environ. 43 (2003) 345.
[11] W.P. Wang, Z.F. Wang, Y. Ding, J.Y. Xi, G.X. Lu, Catal. Lett. 81 (2002) 63.
[12] W.P. Wang, Z.F. Wang, Y. Ding, G.X. Lu, Chem. Res. Chinese U 19 (2003) 206.
[13] J.Y. Xi, Z.F. Wang, W.P. Wang, G.X. Lu, J. Mol. Catal. (China) 15 (2001) 255.
[14] D.K. Liguras, K. Goundani, X.E. Verykios, Int. J. Hydrogen Energy 29 (2004) 419.
[15] D.K. Liguras, K. Goundani, X.E. Verykios, J. Power Sources 130 (2004) 30.
[16] G.A. Deluga, J.R. Salge, L.D. Schmidt, X.E. Verykios, Science 303 (2004) 993.
[17] R.M. Navarro, M.C. Álvarez-Galván, M. Cruz Sánchez-Sánchez, F. Rosa, J.L.G. Fierro, Appl. Catal. B: Environ. 55 (2005) 229.
[18] J. Kugai, S. Velu, C.S. Song, Catal. Lett. 101 (2005) 255.
[19] V. Fierro, O. Akdim, H. Provendier, C. Mirodatos, J. Power Sources 145 (2005) 659.
[20] S. Velu, N. Satoh, C.S. Gopinath, K. Suzuki, Catal. Lett. 82 (2002) 145.
[21] S. Velu, K. Suzuki, M. Vijayaraj, S. Barman, C.S. Gopinath, Appl. Catal. B: Environ. 55 (2005) 287.
[22] J. Kugai, S. Velu, C.S. Song, M.H. Engelhard, Y.H. Chin, J. Catal. 238 (2006) 430.
[23] A. Casanovas, J. Llorca, N. Homs, J.L.G. Fierro, P.R. de la Piscina, J. Mol. Catal. A: Chem. 250 (2006) 44.
[24] J. Llorca, P.R. Piscina de la, J.A. Dalmon, J. Sales, N. Homs, Appl. Catal. B: Environ. 43 (2003) 355.
[25] A.N. Fatsikostas, D.I. Kondarides, X.E. Verykios, Catal. Today 75 (2002) 145.
[26] M. Somani, M.A. Liauw, D. Luss, Chem. Eng. Sci. 51 (1996) 4259.
[27] S. Cavallaro, V. Chiodo, A. Vita, S. Freni, J. Power Sources 123 (2003) 10.
[28] V. Fierro, O. Akdim, C. Mirodatos, Green Chem. 5 (2003) 20.
[29] J.L. Bi, S.N. Hsu, C.T. Yeh, C.B. Wang, Catal. Today, in press.
[30] C.T. Bao, Z. Xu, Q. Ma, J. Hong, H. Sang, D. Sheng, Adv. Mater. 14 (2002) 44.
[31] P.A. Dilara, J.M. Vohs, Surf. Sci. 321 (1994) 8.
[32] P.G.J. Koopman, A.P.G. Kieboom, H.V. Bekkum, J. Catal. 69 (1981) 172.
[33] S. Hosokawa, H. Kanai, K. Utani, Y. Taniguchi, Y. Saito, S. Imamura, Appl. Catal. B: Environ. 45 (2003) 181.
[34] S.H. Park, M.S. Tzou, W.M.H. Sachtler, Appl. Catal. 24 (1986) 85.
[35] C.P. Hwang, C.T. Yeh, J. Catal. 182 (1999) 48.
[36] M. Mavrikakis, M.A. Barteau, J. Mol. Catal. A: Chem. 131 (1998) 135.
[37] C. Diagne, H. Idriss, A. Kiennemann, Catal. Commun. 3 (2002) 565.
[38] S. Cavallaro, V. Chiodo, S. Freni, N. Mondello, F. Frusteri, Appl. Catal. A: Gen. 249 (2003) 119.
[39] R.R. Davda, J.W. Shabaker, G.W. Huber, R.D. Cortright, J.A. Dumesic, Appl. Catal. B: Environ. 56 (2005) 171.
[40] S.H. Oh, R.M. Sinkevitch, J. Catal. 142 (1993) 254.
[41] M. Watanabe, H. Uchida, H. Igarashi, M. Suzuki, Catal. Lett. 47 (1997) 17.
[42] M. Watanabe, H. Igarashi, M. Suzuki, Y. Sasaki, H. Uchida, Appl. Catal. A: Gen. 159 (1997) 159.
[43] M. Echigo, N. Shinke, S. Takami, S. Higashiguchi, K. Hirai, T. Tabata, Catal. Today 84 (2003) 209.
[44] M. Echigo, T. Tabata, Catal. Today 90 (2004) 269.
[45] S.Y. Chin, O.S. Alexeev, M.D. Amiridis, Appl. Catal. A: Gen. 286 (2005) 157.
[46] G. Xu, Z.G. Zhang, J. Power Sources 157 (2006) 64.
[47] Y. Cong, V.V. Spaendonk, R.I. Masel, Surf. Sci. 385 (1997) 246.
[48] Y. Cong, R.I. Masel, Surf. Sci. 396 (1998) 1.
[49] A.R. Garcia, J.L.D. Silva, L.M. Ilharco, Surf. Sci. 415 (1998) 183.
[50] A.F. Lee, D.E. Gawthrope, N.J. Hart, K. Wilson, Surf. Sci. 548 (2004) 200.